



PERGAMON

Deep-Sea Research I 48 (2001) 761–787

DEEP-SEA RESEARCH
PART I

www.elsevier.com/locate/dsr

Modeling redox cycling across the suboxic–anoxic interface zone in the Black Sea

Temel Oguz^{a,*}, James W. Murray^b, Amy E. Callahan^b

^aMiddle East Technical University, Institute of Marine Sciences, P.O. Box 28, Erdemli 33731, Icel, Turkey

^bUniversity of Washington, School of Oceanography, 104 Ocean Teaching Building, Seattle, WA 98195-7940, USA

Received 24 July 1999; received in revised form 20 January 2000; accepted 12 May 2000

Abstract

The reactions controlling the suboxic–anoxic interface structure in the Black Sea are investigated with a prognostic, one-dimensional vertically resolved diffusion-reaction model involving O_2 , NO_3^- , NH_4^+ , HS^- , S^0 , Mn^{2+} , MnO_2 . All reactions are expressed in a second-order form, and values for the rate constants are estimated from laboratory and field measurements made during the 1988 RV *Knorr* expedition. The model successfully simulates the vertical profiles of O_2 , N, S and Mn species in the region between upper and lower boundaries of the model, which were specified at depths corresponding to $\sigma_t \sim 15.50 \text{ kg/m}^3$ and $\sigma_t \sim 16.50 \text{ kg/m}^3$. The model identifies an approximately 30 m thick suboxic layer with oxygen concentrations less than $5 \mu\text{M}$ and zero sulfide concentrations between $\sigma_t \sim 15.55 \text{ kg/m}^3$ and $\sigma_t \sim 16.05 \text{ kg/m}^3$. Dissolved oxygen decreases to trace concentrations above the zone of nitrate reduction. Hydrogen sulfide begins to increase downward into deeper levels of the anoxic pool starting at $\sigma_t \sim 16.0 \text{ kg/m}^3$, where nitrate becomes undetectable. Dissolved manganese and ammonium also increase beneath the suboxic layer. The position at which sulfide concentrations appear coincides with the particulate manganese peak, reflecting the paramount role of manganese cycling in the redox processes. This structure is found to have a fairly persistent character for a wide range of rate constants. Oxidation reactions by oxygen alone are not sufficient to provide a realistic interface structure in the absence of particulate manganese formed by oxidation of Mn^{2+} by NO_3^- . A transient lateral oxygen supply into sulfide rich waters alters the anoxic–suboxic structure by rapidly depleting local sulfide concentrations at the depths of oxygen injection. © 2000 Elsevier Science Ltd. All rights reserved.

Keywords: Redox cycling; Modeling; Suboxic zone; Black Sea

* Corresponding author. Tel.: + 90-324-521-2406; fax: + 90-324-521-2327.
E-mail address: oguz@ims.metu.edu.tr (T. Oguz).

1. Introduction

A distinguishing feature of the Black Sea is the permanent anoxia of the subpycnocline waters. Almost 85% of its total volume is devoid of oxygen at depths below ~ 100 m within the interior part of the basin, and below ~ 150 m around its periphery. Because it is nearly landlocked, ventilation of the deep waters by lateral influxes is relatively poor. In addition, a strong density stratification effectively inhibits vertical mixing. Though once a fresh water lake, the Black Sea has been the largest anoxic basin of the global oceans over the last ~ 7000 yr.

Pump cast measurements performed during the 1988 RV *Knorr* cruises (Murray, 1991) provided high-resolution sampling with minimal contamination. They identified an oxygen-deficient ($O_2 \leq 5 \mu\text{M}$), non-sulfidic layer with a thickness of 10–40 m, called the “Suboxic Layer (SOL)” (Murray et al., 1989). This was contrary to earlier observations in which dissolved oxygen concentrations up to $10 \mu\text{M}$ were measured within the sulfidic layer (Sorokin, 1972; Karl, 1978; Faschuk et al., 1990; Rozanov et al., 1998), suggesting that dissolved oxygen and H_2S could co-exist. Co-existence of oxygen and sulfide is, however, difficult to justify considering the rapid kinetics of their reaction (Millero et al., 1987). Grashoff (1975) was the first to point out that overlapping was an artifact of atmospheric contamination with oxygen during the sampling. More recent observations (Tugrul et al., 1992; Saydam et al., 1993; Buesseler et al., 1994; Ereemeev, 1996; Basturk et al., 1994, 1997, 1998) have supported the existence of the SOL, even though the methodologies used were not as accurate as the pump cast technique employed in the *Knorr* surveys.

All these studies found the SOL to be very stable and reproducible. Analyzing data available since the 1960s, Tugrul et al. (1992) and Buesseler et al. (1994) showed that the suboxic zone existed before the 1988 *Knorr* cruise, but it was not observed because of low sampling resolution and contamination of water samples with atmospheric oxygen. Konovalov et al. (1999) suggested that, while the first appearance of sulfide has been stable, the upper boundary of the SOL may have moved to shallower levels, especially since late 1970s. It was shown to be related to more active organic matter generation-degradation, more active nitrogen cycling, and thus a higher rate of oxygen consumption in the water column. These modifications were caused by intense eutrophication, population explosion of gelatinous carnivores and other opportunistic species in the Black Sea pelagic food web, and subsequently more frequent and longer-lasting phytoplankton blooms during the year (Ivanov and Oguz, 1998).

The origin and maintenance of the SOL and the redox reactions taking place across the anoxic interface are not fully understood and deserve further observational and modeling studies. Based on available data from the Black Sea and other similar basins, several mechanisms have been hypothesized to contribute to the interface structure between the suboxic and anoxic layers (Murray et al., 1995; 1999). The first involves anaerobic sulfide oxidation and nitrogen transformations coupled to the manganese and iron cycles. It was proposed that the upward fluxes of sulfide and ammonium may be oxidized by Mn(III, IV) and Fe(III) species, whereas the downward flux of nitrate may be reduced by dissolved manganese and ammonium. Mn(II) and Fe(II) oxidation and Mn(IV) and Fe(III) reduction are both microbially catalyzed, but dissolved chemical reduction may also play a role in Mn(IV) reduction.

Anoxygenated photosynthesis is also considered as a mechanism of the SOL formation. The reduced chemical species (HS^- , Mn^{2+} , Fe^{2+}) are oxidized by anoxygenic phototrophic bacteria in

association with phototrophic reduction of CO_2 to form organic matter. This mechanism is supported by the discovery of large quantities of bacteriochlorophyll pigments near the suboxic–anoxic boundary (Repeta and Simpson, 1991; Jorgensen et al., 1991; Jannasch et al., 1991). This bacterium is capable of growth using reduced S (H_2S or S^0) at very low light levels ($\ll 0.1\%$ of the incident radiation at the surface). The third mechanism is oxidation of H_2S by oxygen and particulate manganese injected quasi-horizontally into the anoxic layer (Murray et al., 1989; Tebo et al., 1991; Basturk et al., 1998).

All these mechanisms presumably contribute to the redox dynamics at the Black Sea anoxic interface. However, so little is known about the anoxygenic photosynthesis that it is difficult to quantify or include in a substantial way. We also note that the observational support for anoxygenic photosynthesis came from the measurements carried out at three stations within the interior part of the basin during the *Knorr* 1988 expedition (Repeta et al., 1989). The sulfide interface was located around 80–100 m depths at these stations, and thus able to receive sufficient light to maintain bacterial photosynthetic activity. The data, however, indicated a five-fold decrease in the maximum bacteriochlorophyll-e concentrations as the interface deepened from 74 m at one station to 100 m at the other. The concentrations are expected to decrease further as the interface deepens more towards the peripheral zone of the basin, permanently characterized by anticyclonic-dominated circulation (Oguz et al., 1993).

Presence of a persistent suboxic zone structure with its lower boundary located at the depth of around 160–180 m within the quasi-permanent anticyclonic gyre of the eastern basin (Basturk et al., 1997) suggests that anaerobic sulfide oxidation should control first-order dynamics of the redox structure in the Black Sea. Anoxygenated photosynthesis is expected to have an additional contribution to the dissolved oxygen–hydrogen sulfide separation at shallower depths, and thus to formation of somewhat thicker SOL within cyclonic areas of the basin. On the other hand, its mathematical formulation is not straightforward because of uncertainties in the parameterization of processes and specification of a realistic set of values for the parameters. The role of anoxygenic photosynthesis is, therefore, excluded from the model structure described in the present paper.

As opposed to recent advances in the modeling of redox cycling in marine sediments (e.g. Wang and Cappellen, 1996; Soetaert et al., 1996; Boudreau et al., 1998; Jahnke, 1998), model studies dealing with water column redox processes are extremely limited. In the Black Sea, the nitrogen and sulfur cycles were modeled by Yakushev and Neretin (1997) using the sulfide oxidation by oxygen alone, without incorporating the role of nitrogen transformations coupled to the manganese cycle. Sulfur cycling involved abiogenic oxidation to thiosulfate followed by its bacterial oxidation to sulfate by thiobasili. Because this bacterium requires oxygen, sulfur oxidation depends on the availability of oxygen. The lowest oxygen concentration requirement for oxidation was set to 2 μM , and its maximum efficiency was assumed to take place at oxygen concentrations greater than 9 μM . The Yakushev and Neretin model thus requires a continuous supply of oxygen to drive the sulfur cycle. This supply was provided by a downward diffusive oxygen flux using a vertical eddy diffusivity of $1 \times 10^{-5} \text{ m}^2/\text{s}$, which appears to be an order of magnitude higher than those estimated from microstructure measurements and hydrographic data for such strongly stratified conditions (see Section 6). Their simulations therefore show overlapping dissolved oxygen and sulfide concentrations. In Yakushev (1998), this model was extended to incorporate simplified manganese cycling in which particulate manganese used for oxidizing hydrogen sulfide was

produced by oxidation of dissolved manganese with oxygen. Since the manganese cycling depends on the availability of oxygen within the interface zone, this model does not differ conceptually from the previous one, and also cannot explain sulfide oxidation in the absence of oxygen. Another model based on the same concept of sulfide–oxygen interaction was given by Belyaev et al. (1997). This model was developed specifically for the northwestern shelf ecosystem, and a case study of the model implementation was described by Lyubartseva and Lyubartsev (1998).

In this study, we explore basic features of redox cycling across the suboxic–anoxic interface of the Black Sea using a one-dimensional vertically resolved diffusion-reaction model. Specifically, we concentrate on the first and third mechanisms described above, and evaluate whether various proposed redox reactions simulate major observed features of the interface zone. This work complements our earlier models of pelagic food web structure, nitrogen cycling and oxygen production/consumption (Oguz et al., 1996, 1998a,b, 1999).

2. Observed features of the SOL structure

The data collected by the RV *Knorr* surveys during the spring–summer 1988 are regarded as the best available and most complete data set acquired to date in the Black Sea. The vertical distributions of O_2 , NO_3^- , NH_4^+ , HS^- , S^0 , Mn^{2+} , MnO_2 at station BS3-6 located within the central part of the western basin ($43^\circ N$, $34^\circ E$) during 13 June 1988 are plotted in Fig. 1. For more detailed descriptions of the biogeochemical features of the SOL, we refer to papers by Codispoti et al. (1991); Lewis and Landing, (1991), Tebo (1991) and Nealson et al. (1991). Other independent measurements performed during the 1990s (Basturk et al., 1994, 1997, 1998; Gokmen et al., 1998; Konovalov et al., 1997) showed very similar structures and indicated stability of the system during the last decade.

Features of the vertical biogeochemical structure in the Black Sea always correspond to distinct density surfaces, even if they may be located at different depths depending on local circulation (Vinogradov and Nalbandov, 1990; Tugrul et al., 1992; Saydam et al., 1993; Basturk et al., 1994, 1997). This is because the SOL lies within the very strong and stable permanent pycnocline (Fig. 1a) with a density difference of more than $\sigma_t \sim 2.0 \text{ kg/m}^3$ across this zone. It is therefore customary to express vertical biogeochemical variations in terms of sigma- t , rather than depth.

Two distinct oxygen variations are evident around the upper boundary of the SOL in Fig. 1b. The steeper slope of the oxygen profile down to $\sigma_t \sim 15.55 \text{ kg/m}^3$ reflects intense oxygen consumption during oxidation of organic matter. At deeper levels, oxygen concentration stays below $5 \mu M$. For example, it is about $3 \mu M$ at $\sigma_t \sim 15.87 \text{ kg/m}^3$, followed by the value of $0.5 \mu M$ at $\sigma_t \sim 15.98 \text{ kg/m}^3$ at a depth of 95 m. On the other hand, the first appearance of hydrogen sulfide occurs at $\sigma_t \sim 16.15 \text{ kg/m}^3$ at 106 m. Thus, the thickness of the suboxic layer is about 10 m if $1 \mu M$ dissolved oxygen level (a typical limit of accuracy of the colorimetric method in the *Knorr* 1988 measurements) is accepted as its upper boundary. When $5 \mu M$ is considered as a typical detection limit of dissolved oxygen measured by the conventional Winkler method during the *Knorr* 1988 surveys, the upper boundary of the SOL is defined around $\sigma_t \sim 15.6 \text{ kg/m}^3$ located at 75 m. Its thickness is then about 30 m. There is no formal definition of the suboxic layer in the Black Sea but,

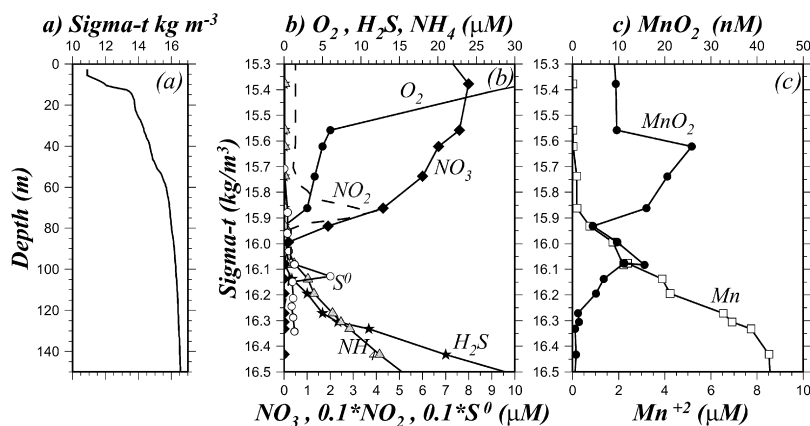


Fig. 1. (a) Depth profile of density for the upper 150 m water column, (b) O_2 , HS^- , NH_4^+ , NO_3^- , NO_2^- , S^0 profiles, and (c) Mn^{2+} , MnO_2 profiles plotted versus density (σ_t) for station BS3-6 (43°N , 34°E) during RV *Knorr* survey of 13 June 1988.

according to the *Knorr* data set, the upper and lower boundaries of the SOL were suggested to lie along the density surfaces of $\sigma_t \sim 15.55 \pm 0.05$ and $16.15 \pm 0.05 \text{ kg/m}^3$ (Murray, 1991). The upper boundary also coincides approximately with the maximum nitrate concentrations of $\sim 6\text{--}9 \mu\text{M}$ (Fig. 1b). Both the position and magnitude of the nitrate peak seem to be maintained at constant values since the 1980s. Due to excess anthropogenic nitrate input relative to losses to the atmosphere and deep layer, there has been a continuous increase of the peak concentrations from $2\text{--}3 \mu\text{M}$ during the 1960s to $6\text{--}8 \mu\text{M}$ in the 1980s and $7\text{--}9 \mu\text{M}$ in the 1990s (Tugrul et al., 1992; Basturk et al., 1997; Konovalov et al., 1999).

The strong stability of the upper layer water column does not permit ventilation of the SOL even during periods of winter convective overturning (Oguz et al., 1998a). In the absence of oxygen, organic matter decomposition proceeds via denitrification, as suggested by a sharp decrease in nitrate concentration to trace values ($\sim 0.1 \mu\text{M}$) at $\sigma_t \sim 16.0 \text{ kg/m}^3$. The presence of a narrow nitrite peak of $0.2\text{--}0.4 \mu\text{M}$ centered at approximately $\sigma_t \sim 15.85 \text{ kg/m}^3$ is another signature of denitrification. Similarly, NH_4^+ , HS^- and Mn^{2+} concentrations also decrease upward towards $\sigma_t \sim 16.0 \text{ kg/m}^3$ from their pools in the deeper part of the water column. In particular, we note pronounced decrease in HS^- concentrations around $\sigma_t \sim 16.1 \text{ kg/m}^3$. NH_4^+ and Mn^{2+} profiles follow similar trends with slightly different slopes and disappear, respectively, near $\sigma_t \sim 16.0 \text{ kg/m}^3$ and $\sigma_t \sim 15.9 \text{ kg/m}^3$. Peaks of S^0 and MnO_2 form around $\sigma_t \sim 16.1 \text{ kg/m}^3$ as by-products of sulfur and manganese cycling.

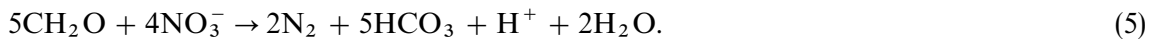
Overall, Fig. 1 displays general features of a marine redox cycling between the suboxic and anoxic layers. Dissolved oxygen decreases below detection limits above a zone of nitrate reduction. Dissolved manganese and ammonium begin to increase coincidentally at the base of the SOL, followed by an increase in sulfide concentration. Marked gradients of particulate manganese around the transition zone reflect the role of manganese cycling as proposed and studied by Spencer and Brewer (1971), Brewer and Spencer (1974), Kempe et al. (1991), Tebo (1991), Tebo et al. (1991), and Lewis and Landing (1991).

3. Redox reactions

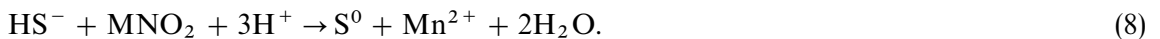
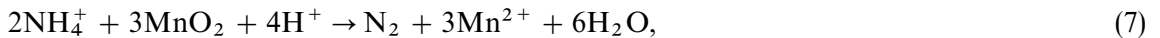
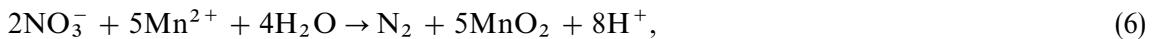
The model presented in this study considers simplified nitrogen and sulfur cycles catalyzed by the manganese cycle across the suboxic–anoxic interface zone. In the presence of oxygen, the redox reactions suggested by Murray et al. (1995) include oxidation of particulate organic matter, hydrogen sulfide, ammonium and dissolved manganese by dissolved oxygen. These reactions are



In the absence of oxygen, heterotrophic denitrification follows the reaction



Eq. (5) is a simplified form of the two step reactions involving an intermediate step of nitrite oxidation/reduction. It, therefore, does not reproduce the nitrite peak observed near the base of the SOL (see Fig. 1b). In oxygen depleted waters, Murray et al. (1995) suggested the following oxidation–reduction reactions via manganese cycling:



Accordingly, dissolved manganese (Mn^{2+}) reacts with nitrate (NO_3^-) to produce settling particulate manganese (MnO_2) and nitrogen gas (N_2). HS^- and ammonium (NH_4^+) transported upwards from deeper levels are oxidized by MnO_2 to form elemental sulfur (S^0), N_2 and Mn^{2+} . S^0 is reduced back to HS^- by bacteria (Myers and Nealson, 1988), N_2 escapes to the atmosphere whereas dissolved manganese produced locally is re-oxidized by nitrate.

Oxidation of Mn^{2+} by NO_3^- (Reaction (6)) is based on free energy, ΔG_f , calculations and the water column distributions. ΔG_f is negative at in situ concentrations (see Murray et al., 1995) but it is low. There is no direct evidence for this reaction to occur in the Black Sea, and it is therefore strictly a hypothesis at present, even though many sediment studies have suggested its occurrence (e.g. Shaw et al., 1990; Schultz et al., 1994; Luther III et al., 1997; Aller et al., 1998; Hulth et al., 1999). Luther III et al. (1997) also suggested that the upward flux of NH_4^+ can be oxidized by MnO_2 to form N_2 and Mn^{2+} (Reaction (7)). The reaction of MnO_2 with HS^- is well known (Burdige and Nealson, 1986).

The reactions given by Eqs. (2)–(8) avoid modeling the intermediate steps of the sulfur cycle (e.g. $\text{S}_2\text{O}_3^{2-}$), and thus H_2S generation through the sulfate reduction process. Local sulfate reduction appears to be of secondary importance with respect to its supply from deeper levels by diffusion (c.f. Yakushev and Neretin, 1997). Heterotrophic processes such as ammonification and nitrification take place primarily in more oxygenated parts of the water column above the suboxic zone, and therefore are not considered in our model.

The reactions related with the iron cycle are also not included, for simplicity. Dissolved iron concentrations are typically an order of magnitude smaller than those of dissolved manganese in the Black Sea (Lewis and Landing, 1991). A similar order of magnitude difference also exists between their electron-equivalent gradients (Murray et al., 1995). Therefore, it is reasonable to neglect, to a first approximation, the contribution of the iron cycle on the Black Sea redox dynamics. All these assumptions and idealizations are believed to have secondary contributions to redox cycling processes, and help to simplify the problem to a more tractable form with fewer reactions.

Eqs. (1)–(8) form a coupled and highly interactive system. We note that this set of reactions does not provide a closed redox cycle; it indicates a continuous loss of nitrogen in the form of N_2 gas to the atmosphere, and thus requires a continuous supply of NO_3^- into the redox layer to oxidize dissolved manganese diffusing there from deeper levels. The nitrate supply is provided continuously by downward diffusion from the nitracline zone where nitrate concentrations yield a maximum of around 6–9 μM (see Fig. 1b).

4. Reaction kinetics

The kinetics of reactions given in Eqs. (1)–(8) are not well known in terms of the values of the rate constants and functional dependencies. Thus, the kinetic expressions are postulated to be first order with respect to each of the individual state variables. Then, they are expressed by

$$R_1 = k_1 f_n(O_2)[O_2], \quad (9)$$

$$R_2 = k_2 [HS^-][O_2], \quad (10)$$

$$R_3 = k_3 [NH_4^+][O_2], \quad (11)$$

$$R_4 = k_4 [Mn^{2+}][O_2], \quad (12)$$

$$R_5 = k_5 f_d(O_2)[NO_3^-], \quad (13)$$

$$R_6 = k_6 [NO_3^-][Mn^{2+}], \quad (14)$$

$$R_7 = k_7 [NH_4^+][MnO_2], \quad (15)$$

$$R_8 = k_8 [HS^-][MnO_2], \quad (16)$$

where k_i 's denote rate constants, whose definitions and ranges of values are given in Table 1. $f_n(O_2)$ and $f_d(O_2)$ represent, respectively, oxygen dependence of remineralization and denitrification rates. $f_n(O_2)$ is taken to be equal to one for oxygen concentrations exceeding 5 μM , and zero otherwise. $f_d(O_2)$ is set to zero when $O_2 \geq 5 \mu M$ and to one otherwise. A threshold oxygen concentration of 5 μM seems to be a reasonable choice based on available observations (e.g. Lipschultz et al. (1990); see also Yakushev and Neretin (1997)), which report a range of values between 2 and 7 μM in different oceanic regions. Our sensitivity experiments indicated that turning off aerobic respiration at 5 μM was not critical for the model results.

As implied by Eqs. (9) and (13), the model does not include labile organic matter as an independent prognostic variable. The reaction kinetics (1) and (5) are thus expressed independent of

Table 1
Definition of model parameters and their range of values

Parameter	Definition	Range
k_1	Remineralization rate	0.1–1.0 1/d Ward and Kilpatrick (1991)
k_2	Rate of sulfide oxidation by O_2	0.01–1.0 $\mu\text{M}^{-1} \text{d}^{-1}$ Millero (1991)
k_3	Rate of ammonium oxidation by O_2 (nitrification rate)	0.01–0.1 $\mu\text{M}^{-1} \text{d}^{-1}$ Ward and Kilpatrick (1991)
k_4	Rate of manganese oxidation by O_2	0.01–0.1 $\mu\text{M}^{-1} \text{d}^{-1}$ Tebo (1991)
k_5	Denitrification rate	0.001 d^{-1} Ward and Kilpatrick (1991)
k_6	Rate of manganese oxidation by NO_3^-	0.01–0.1 $\mu\text{M}^{-1} \text{d}^{-1}$ Tebo (1991)
k_7	Rate of ammonium oxidation by MnO_2	0.1–20.0 $\mu\text{M}^{-1} \text{d}^{-1}$ Ward and Kilpatrick (1991)
k_8	Rate of sulfide oxidation by MnO_2	1–100 $\mu\text{M}^{-1} \text{d}^{-1}$ Yao and Millero (1993) Lewis and Landing (1991)
k_9	Sulphide reduction rate	0.01–0.1 d^{-1} Yakushev and Neretin (1997)
W_s	Sinking rate of particulate manganese	1.0–10 m/d Yakushev (1998)
A_v	Kinematic diffusivity	$1 - 7 \times 10^{-6} \text{ m}^2/\text{s}$ Gregg and Ozsoy (1999) Gargett (1984)

organic matter concentration, implying that it is not a limiting factor for these reactions. At present this is a simplification we are forced to make since there is very little POC data available for the Black Sea. Karl and Knauer (1991) provided some POC measurements which, however, did not have enough detail in their vertical structure. Moreover, the linear form of Eqs. (9) and (13) is an approximation to its more general Monod-type hyperbolic representation for small concentrations of dissolved oxygen and nitrate in the suboxic layer.

5. Diffusion-reaction equations

The diffusion-reaction equations describing the processes given above are

$$\frac{\partial[\text{O}_2]}{\partial t} = \frac{\partial}{\partial z} \left(A_v \frac{\partial[\text{O}_2]}{\partial z} \right) - R_1 - \frac{1}{2}R_2 - 2R_3 - \frac{1}{2}R_4 + F_L(\text{O}_2), \quad (17)$$

$$\frac{\partial[\text{HS}^-]}{\partial t} = \frac{\partial}{\partial z} \left(A_v \frac{\partial[\text{HS}^-]}{\partial z} \right) - R_2 - R_8, \quad (18)$$

$$\frac{\partial[\text{S}^0]}{\partial t} = R_2 + R_8 - k_9[\text{S}^0], \quad (19)$$

$$\frac{\partial[\text{NO}_3^-]}{\partial t} = \frac{\partial}{\partial z} \left(A_v \frac{\partial[\text{NO}_3^-]}{\partial z} \right) - R_5 - \frac{2}{5}R_6 + R_3, \quad (20)$$

$$\frac{\partial[\text{NH}_4^+]}{\partial t} = \frac{\partial}{\partial z} \left(A_v \frac{\partial[\text{NH}_4^+]}{\partial z} \right) - R_7 - R_3, \quad (21)$$

$$\frac{\partial[\text{N}_2]}{\partial t} = \frac{\partial}{\partial z} \left(A_v \frac{\partial[\text{N}_2]}{\partial z} \right) + \frac{1}{2}R_5 + \frac{1}{5}R_6 + \frac{1}{2}R_7, \quad (22)$$

$$\frac{\partial[\text{Mn}^{2+}]}{\partial t} = \frac{\partial}{\partial z} \left(A_v \frac{\partial[\text{Mn}^{2+}]}{\partial z} \right) - R_4 - R_6 + \frac{3}{2}R_7 + R_8, \quad (23)$$

$$\frac{\partial[\text{MnO}_2]}{\partial t} = W_s \frac{\partial[\text{MnO}_2]}{\partial z} - \frac{3}{2}R_7 - R_8 + R_4 + R_6, \quad (24)$$

where t is time, z is the vertical coordinate, ∂ denotes partial differentiation. The first terms on the right-hand sides of the equations (except Eq. (24)) represent vertical diffusion. The fractions represent the stoichiometries in Eqs. (1)–(8). $F_L(\text{O}_2)$ in Eq. (17) parameterizes the lateral advective flux of oxygen included in one of the experiments to investigate the role of lateral injections from the shelf break zone on the structure of the suboxic–anoxic interface zone. W_s denotes the sinking rate of MnO_2 particles. The contribution of vertical advective motion on redox cycling is neglected, since parameterization of vertical advective velocity is questionable in the case of one-dimensional, non-divergent flow conditions.

Eqs. (17)–(24) were solved numerically by the finite differencing procedure over a 75 m thick water column covering the suboxic–anoxic interface zone. The system of equations was discretized by introducing 25 depth levels, implying a 3 m vertical grid spacing. A time step of 10 min was used during integration of the equations. The numerical solution procedure follows principally that given in Oguz et al. (1996) describing a coupled physical-biogeochemical model based on the one-dimensional implementation of the Princeton Ocean Model (c.f. Mellor, 1990). The time derivatives were discretized by Leapfrog differencing. The diffusion terms, together with some of the reaction terms in each of the equations, were treated implicitly to maintain stability of the solution. This solution procedure is quite general and has wide-spread applicability for such diffusion-reaction systems (e.g. Soetaert et al., 1996; Boudreau, 1996). The numerical solution methods were first verified by an analytical solution using a simplified system involving only the oxygen and hydrogen sulfide reactions. The details of the analytical solution follow that presented by Eremeev (1996, Chapter 3).

For a typical density profile (Fig. 1a) representative of interior Black Sea conditions, the upper boundary was located at the depth of ~ 75 m. This position corresponds approximately to the base of the upper nitracline/oxycline zone at $\sigma_t \sim 15.5$ kg/m^3 (Fig. 1b). The lower boundary was located at the depth of 150 m coinciding roughly with $\sigma_t \sim 16.5$ kg/m^3 . The model was forced by prescribed constant nitrate and oxygen concentrations at the upper boundary, and hydrogen sulfide, ammonium and dissolved manganese concentrations at the lower boundary; otherwise the

Table 2
Conditions prescribed at the upper and lower boundaries of the model

Variable	Surface	Bottom
[O ₂]	10 μM	$A_v[\text{O}_2]_z = 0$
[NO ₃ ⁻]	8 μM	$A_v[\text{NO}_3]_z = 0$
[NH ₄ ⁺]	$A_v[\text{NH}_4]_z = 0$	12 μM
[H ₂ S]	$A_v[\text{H}_2\text{S}]_z = 0$	25 μM
[Mn ²⁺]	$A_v[\text{Mn}^{2+}]_z = 0$	8 μM
[MnO ₂]	$W_s[\text{MnO}_2] = 0$	$W_s[\text{MnO}_2] = -A_v[\text{Mn}^{2+}]_z$

vertical diffusive fluxes were set to zero at the boundaries. A summary of the boundary conditions is given in Table 2.

The values of all variables were set initially to zero. The model therefore assumed no prescribed initial structure. The system approaches its statistical equilibrium state after a few years of transient adjustment in response to forcings from the upper and lower boundaries. The results presented here correspond to the end of the fifth year, in which all fields attain their steady-state values except MnO₂. MnO₂ concentrations still tend to exhibit slight changes in the narrow suboxic–anoxic interface zone. These variations are however small (less than ~ 10% of the maximum concentrations), and therefore we will consider the system to be in a quasi-equilibrium state.

6. Estimation of parameter values and model calibration

Microstructure measurements (Gregg and Ozsoy, 1999) suggest a small vertical diffusion coefficient, A_v , on the order of 10^{-6} m²/s, for the region of the suboxic zone. A similar value can also be obtained from Gargett's (1984) parameterization expressed by $A_v = aN^{-q}$, where a is a constant with a typical value of $\sim 1 \times 10^{-3}$ cm²/s², N the square root of the Brunt-Vaisala frequency [$N \equiv -(g/\rho_0^{-1})(\partial\rho/\partial z)$]^{1/2} and q a constant varying between 0.5 and 1. For typical winter and summer stratifications, the Gargett (1984) formula yields an almost uniform vertical structure with values of A_v between 0.7×10^{-6} m²/s (for $q = 0.5$) and 7.0×10^{-6} m²/s (for $q = 1.0$) for the suboxic–anoxic interface region, i.e. below 75 m depth in Fig. 2. Furthermore, Brewer and Spencer (1974) estimated A_v in the interface region as 1.4×10^{-6} m²/s from oxygen budget computations. In our standard experiment, we assumed a constant value of $A_v = 2 \times 10^{-6}$ m²/s, but we carried out a set of sensitivity experiments using different values to evaluate its effect on the biogeochemical structure of the water column. Some of these experiments will be described below.

Ward and Kilpatrick (1991) measured nitrate reduction and ammonium oxidation rates by ¹⁵N tracer addition during the 1988 Knorr expedition. The nitrate reduction rate in the suboxic zone ranged from 0.6 to 6.0 nM/d with nitrate concentrations between 2 and 8 μM. If all nitrate reduction can be attributed to heterotrophic denitrification, then k_5 is roughly 0.001 d⁻¹. Similarly, the ammonium oxidation (i.e. nitrification) rate measured was 10–100 nM/d. With ammonium and oxygen concentrations around 1.0 μM near the suboxic–anoxic interface zone, k_3 falls in the range 0.01–0.1 μM⁻¹ d⁻¹. The same ammonium oxidation rates are also used to estimate the rate

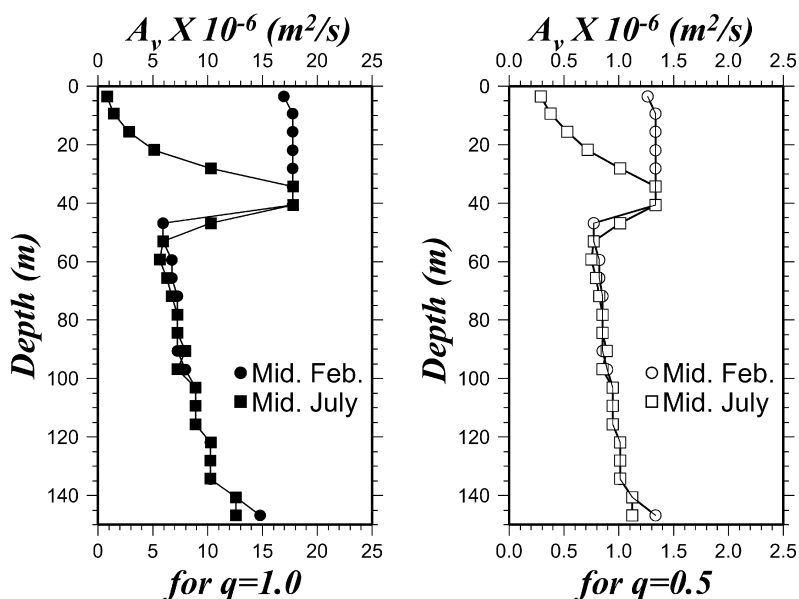


Fig. 2. Depth profiles of the vertical diffusion coefficient computed from Gargett's (1984) formula with two different values of q : for $q = 1.0$ on the left with solid symbols, and $q = 0.5$ on the right with open symbols. Each figure contains two profiles computed for typical vertical density structure of mid-winter and mid-summer.

constant for ammonium oxidation by MnO_2 . Assuming particulate manganese concentrations of 5–25 nM (Lewis and Landing, 1991), k_7 is $\sim 0.1\text{--}20 \mu\text{M}^{-1} \text{d}^{-1}$.

Millero (1991) reported half-lives for sulfide oxidation by oxygen between 1.2 and 2.9 h. Gokmen et al. (1998) provided a similar range of values between 1.3 and 3.4 h. Assuming oxygen concentrations do not change appreciably during the rate measurement, the second-order rate constant k_2 is approximately $0.01\text{--}0.1 \mu\text{M}^{-1} \text{d}^{-1}$. Jorgensen et al. (1991) showed sulfide oxidation rates up to $1\text{--}2 \mu\text{M}^{-1} \text{d}^{-1}$ at the interface zone. Incubation experiments with sterilized particulate matter from this depth suggested that particulate manganese might be involved in this reaction. Assuming MnO_2 concentrations between 2 and 20 nM (Lewis and Landing, 1991), and sulfide concentrations between 5 and $10 \mu\text{M}^{-1}$, the value of k_8 can be estimated in the range $10\text{--}100 \mu\text{M}^{-1} \text{d}^{-1}$. This estimate is however higher than the rate determined in laboratory measurements of hydrogen sulfide oxidation by manganese dioxide (Yao and Millero, 1993). The data of Yao and Millero (1993) suggest a rate of $k_8 \sim 1 \mu\text{M}^{-1} \text{d}^{-1}$. Tebo (1991) measured suboxic manganese oxidation by oxygen at a maximum rate of $0.1 \mu\text{M}/\text{d}$. This implies that k_6 and k_4 can attain maximum values of $0.1 \mu\text{M}^{-1} \text{d}^{-1}$.

Our calibration exercise is not aimed at providing the best possible fits to concentration versus depth profiles for a specific data set. The model calibration proceeds by adjusting parameter values so as to mimic the observed structure similar to the one shown in Figs. 1b and c. This procedure allows production of a parameter set for the so-called “standard experiment” in the following section. Some of these parameters are then varied to systematically explore the role of various reactions on the structure of the suboxic–anoxic interface zone.

7. Model results and discussion

7.1. Experiments without manganese cycling

Before describing the role of the full set of reactions (1)–(8) on the formation of the suboxic zone structure, we first present results from a simplified diffusion-reaction system in which manganese cycling does not take part in the oxidation process. This system involves only Reactions (1)–(3), implying that hydrogen sulfide and ammonium are oxidized by dissolved oxygen. The corresponding kinetic expressions are given by R_1 , R_2 and R_3 in Eqs. (9)–(11). The rate parameters k_4 , k_5 , k_6 , k_7 , k_8 , are set to zero, and Eqs. (23) and (24) describing the temporal changes of Mn^{2+} and MnO_2 are removed from the system of equations. This is similar to the approach followed by Yakushev and Neretin (1997).

The vertical profiles of O_2 and H_2S concentrations representing equilibrium solutions at the end of five years of integration are shown in Figs. 3a and b for two different choices of k_2 , 0.5 and $0.01 \mu\text{M}^{-1} \text{d}^{-1}$. The values of other parameters are listed in Table 3 for Experiments 1A and B. Figs. 3a and b contain two different oxygen and H_2S profiles corresponding with two choices of A_v : 2.0 and $5.0 \times 10^{-6} \text{ m}^2/\text{s}$. For these profiles and for the rest of the paper, the vertical distributions are plotted versus density for comparison with Fig. 1 and to be compatible with observations reported elsewhere, even though they are solved as a function of depth. The profiles will be shown only between the sigma- t levels of 15.5 and 16.4 kg/m^3 . For both values of A_v , the oxygen concentrations are shown to decrease abruptly to $5 \mu\text{M}$ near $\sigma_t \sim 15.55 \text{ kg/m}^3$ from its boundary value of $10 \mu\text{M}$ prescribed at $\sigma_t \sim 15.50 \text{ kg/m}^3$. Such sharp reduction is due to oxygen consumption by aerobic organic matter decomposition (i.e. Reaction (1)), whose rate constant is set to $k_1 = 0.4 \text{ d}$ at oxygen concentrations greater than $5 \mu\text{M}$, and zero otherwise. Below $\sigma_t \sim 15.55 \text{ kg/m}^3$, oxygen concentrations decrease almost linearly towards zero for both cases.

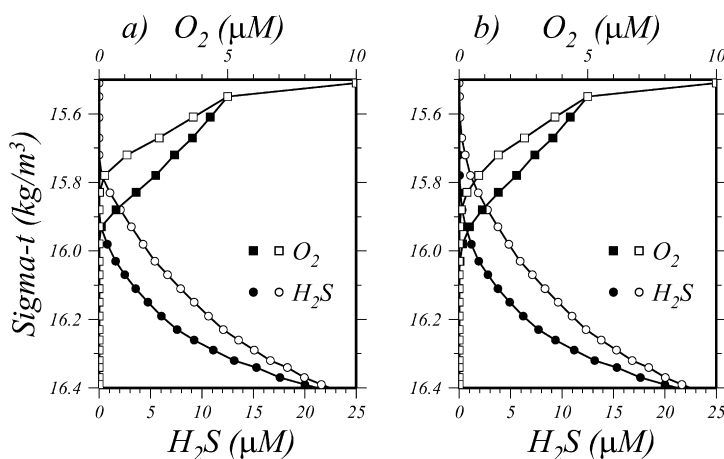


Fig. 3. O_2 , HS^- profiles plotted versus σ_t in the absence of manganese cycling for two different choices of k_2 as (a) $0.5 \mu\text{M}^{-1} \text{d}^{-1}$ (Experiment 1A), and (b) $0.01 \mu\text{M}^{-1} \text{d}^{-1}$ (Experiment 1B). Each figure contains two different O_2 and H_2S profiles using $A_v = 2 \times 10^{-6} \text{ m}^2/\text{s}$ (with solid symbols), and $A_v = 5 \times 10^{-6} \text{ m}^2/\text{s}$ (with open symbols).

For the case $k_2 = 0.5 \mu\text{M}^{-1} \text{d}^{-1}$ (Fig. 3a), zero oxygen concentrations occur near $\sigma_t \sim 15.9 \text{ kg/m}^3$ for $A_v = 2 \times 10^{-6} \text{ m}^2/\text{s}$ (the curve with solid squares), and near $\sigma_t \sim 15.8 \text{ kg/m}^3$ for $A_v = 5 \times 10^{-6} \text{ m}^2/\text{s}$ (the curve with open squares). On the other hand, for both choices of the diffusion coefficient, H_2S penetrates up to the zero oxygen level. H_2S can diffuse towards upper levels with the choice of a higher diffusion coefficient, and therefore gives rise to more oxygen consumption within the suboxic layer. An important point in these plots is to note that both oxygen and hydrogen sulfide vanish at the same position in the water column. This indicates that both vertical diffusion and oxidation reactions almost equally contribute to the temporal changes of the oxygen and hydrogen sulfide.

Fig. 3b displays the results with the rate constant $k_2 = 0.01 \mu\text{M}^{-1} \text{d}^{-1}$. When compared with the previous experiment, oxidation of hydrogen sulfide now proceeds at a slower rate than vertical diffusion. Thus, hydrogen sulfide penetrates more favorably into the oxygenated part of the water column due to vertical diffusion, and consequently oxygen and hydrogen sulfide concentrations overlap to some extent. As expected, overlapping is slightly more pronounced for the case of higher vertical diffusivity. We however note that the overlap is not as large as reported observationally (e.g. Faschuk et al., 1990), and occurs only at oxygen and sulfide concentrations less than $1.0 \mu\text{M}^{-1}$.

7.2. Experiments with partially active manganese cycling

The previous model was modified slightly to incorporate an additional contribution of manganese cycling to the hydrogen sulfide oxidation process using dissolved oxygen as a primary oxidizer. The model now includes diffusion of dissolved manganese from deep waters into the suboxic zone, where it is also oxidized by oxygen (Reaction (4)). Particulate manganese is then produced and used as an additional oxidizer for H_2S (Reaction (8)). The corresponding reaction kinetics R_4 and R_8 are added to the previous set of reactions. This set resembles the model presented by Yakushev (1998). For the choice of parameters given for Experiment 2A in Table 3, the H_2S and O_2 profiles are presented as open symbols in Fig. 4a. These profiles are almost identical with those of the Experiment 1B (with $A_v = 2 \times 10^{-6} \text{ m}^2/\text{s}$ and $k_2 = 0.05 \mu\text{M}^{-1} \text{d}^{-1}$), superimposed on the same figure by the profiles with solid symbols. Furthermore, one order of magnitude increase in the value of k_4 (i.e., $k_4 = 1.0 \mu\text{M}^{-1} \text{d}^{-1}$; see the list of parameters for the Experiment 2B in Table 3), as well as both in the values of k_4 and k_8 (i.e., $k_8 = 250 \mu\text{M}^{-1} \text{d}^{-1}$; see Experiment 2C in Table 3), do not also change this structure (Figs. 4b and c). These experiments indicate that additional contribution of such partially active manganese cycling cannot modify the hydrogen sulfide-oxygen structure within the suboxic zone. Dissolved oxygen still plays the dominant role as sulfide oxidizer as compared with particulate manganese.

7.3. The standard experiment: fully active manganese cycling

Fully active manganese cycling introduces additional particulate manganese by oxidation of dissolved manganese with nitrate (Reaction (6)). For the parameter values of Experiment 3 (Table 3), the vertical structure of the suboxic–anoxic interface region is displayed in Fig. 5. The O_2 and H_2S profiles exhibit several important differences when compared with Fig. 4a. In particular, the H_2S profile approaches trace concentrations at $\sigma_t \sim 16.05 \text{ kg/m}^3$, which is located almost $\sigma_t \sim 0.1 \text{ kg/m}^3$ deeper. Instead of oxygen, the trace H_2S concentrations coincide with those of

Table 3
The values of model parameters used in the experiments

Exp. No.	k_1	k_5	k_9	k_2	k_3	k_4	k_6	k_7	k_8	W_s	A_v	Fig. No.
Standard set	0.4	0.001	0.05	0.01	0.05	0.1	0.05	0.1	50	3.0	0.02	
1A	0.4	0.001	0.05	0.5	0.05	0.0	0.0	0.0	0.0	3.0	0.02, 0.05	Fig. 3a
1B	0.4	0.001	0.05	0.01	0.05	0.0	0.0	0.0	0.0	3.0	0.02, 0.05	Fig. 3b
2A	0.4	0.001	0.05	0.01	0.05	0.1	0.0	0.1	50.0	3.0	0.02	Fig. 4a
2B	0.4	0.001	0.05	0.01	0.05	1.0	0.0	0.1	50.0	3.0	0.02	Fig. 4b
2C	0.4	0.001	0.05	0.01	0.05	1.0	0.0	0.1	250.0	3.0	0.02	Fig. 4c
3, 5	0.4	0.001	0.05	0.01	0.05	0.1	0.05	0.1	50.0	3.0	0.02	Figs. 5, 8
4	0.4	0.001	0.05	0.0	0.0	0.0	0.05	0.1	50.0	3.0	0.02	Fig. 7
6A	0.4	0.001	0.05	0.0	0.0	0.0	1.0	0.1	500.0	3.0	0.02	Fig. 9a
6B	0.4	0.001	0.05	0.0	0.0	0.0	1.0	10.0	500.0	3.0	0.02	Fig. 9b
6K	0.4	0.001	0.05	0.01	0.05	0.1	0.05	0.1	1.0	3.0	0.02	Fig. 10a
6L	0.4	0.001	0.05	0.0	0.0	0.0	0.05	0.1	1.0	3.0	0.02	Fig. 10b
7A	0.4	0.001	0.05	0.01	0.05	0.1	0.05	0.1	50.0	3.0	0.04	Fig. 11a
7B	0.4	0.001	0.05	0.01	0.05	0.1	0.05	0.1	50.0	9.0	0.04	Fig. 11b
7C	0.4	0.001	0.05	0.01	0.05	0.1	0.05	0.1	50.0	9.0	0.06	Fig. 11c

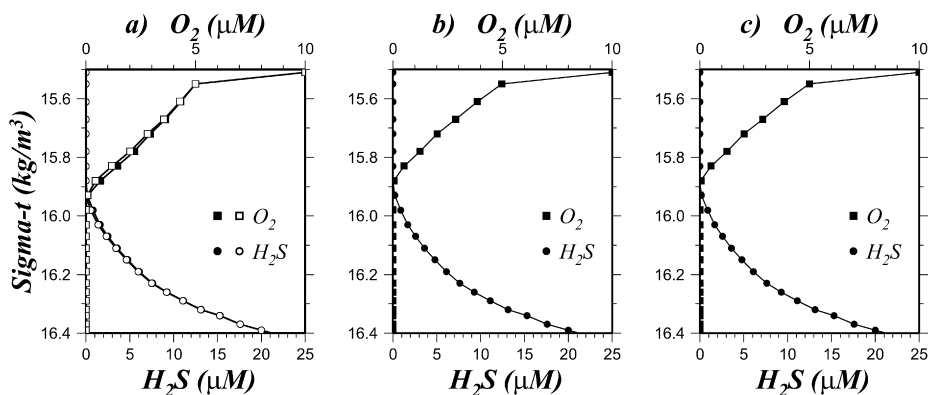


Fig. 4. O_2 , HS^- profiles plotted versus σ_t in the case of partially active manganese cycling (with solid symbols) for (a) $k_4 = 0.1 \mu M^{-1} d^{-1}$ (Experiment 2A), (b) $k_4 = 1.0 \mu M^{-1} d^{-1}$ (Experiment 2B), and (c) $k_4 = 1.0$ and $k_8 = 250 \mu M^{-1} d^{-1}$ (Experiment 2C). Superimposed on Fig. 4a are O_2 and H_2S profiles (with open symbols) shown in Fig. 3a for comparison.

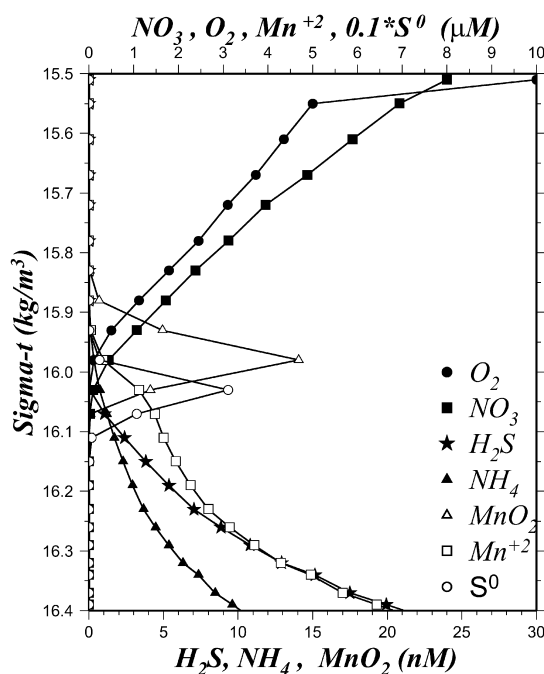


Fig. 5. O_2 , HS^- , NH_4^+ , NO_3^- , S^0 , Mn^{2+} and MnO_2 profiles plotted versus σ_t for the standard experiment (Experiment 3) with fully active manganese cycling.

nitrate, suggesting that NO_3^- consumption controls the H_2S oxidation process even though there is no explicit reaction of $HS^- + NO_3^-$ included. H_2S is mainly oxidized by NO_3^- through MnO_2 at slightly deeper levels. Oxygen consumption thus becomes of secondary importance near the anoxic interface, and dissolved oxygen is thus allowed to diffuse to a slightly deeper level of $\sigma_t \sim 16.0 \text{ kg/m}^3$. The model predicts a suboxic layer characterized by oxygen concentrations less than $5 \mu\text{M}$ and zero hydrogen sulfide concentrations between $\sigma_t \sim 15.55$ and 16.05 kg/m^3 , levels corresponding with the depths of 80 and 110 m (Fig. 1a). Inside this zone, oxygen and sulfide are separated by a null zone of about 5 m. This zone coincides with maximum elemental sulfur concentrations of $0.3 \mu\text{M}$ (Fig. 5).

As H_2S is depleted at the level of vanishing NO_3^- concentrations, ammonium and dissolved manganese diffuse up to the density level of zero oxygen concentration. Contrary to a uniformly decreasing NH_4^+ concentrations, a change in the slope of the dissolved manganese profile between 16.0 and 16.1 kg/m^3 density surfaces reflects additional dissolved manganese production due to manganese cycling. A notable feature of the manganese cycling is the presence of a particulate manganese peak of about 15 nM near the 16.0 kg/m^3 sigma- t level. All these features agree well with the observations shown in Figs. 1b and c.

The relative contributions of the individual reaction terms to the mass balances of H_2S , O_2 , Mn^{2+} , NO_3^- , NH_4^+ concentrations are shown in Fig. 6. In the interface region the oxygen balance (Fig. 6a) is mainly between the vertical diffusion source and sinks due to ammonium and dissolved manganese oxidation ((3) and (4)). The oxygen sink due to hydrogen sulfide oxidation (2) is an order

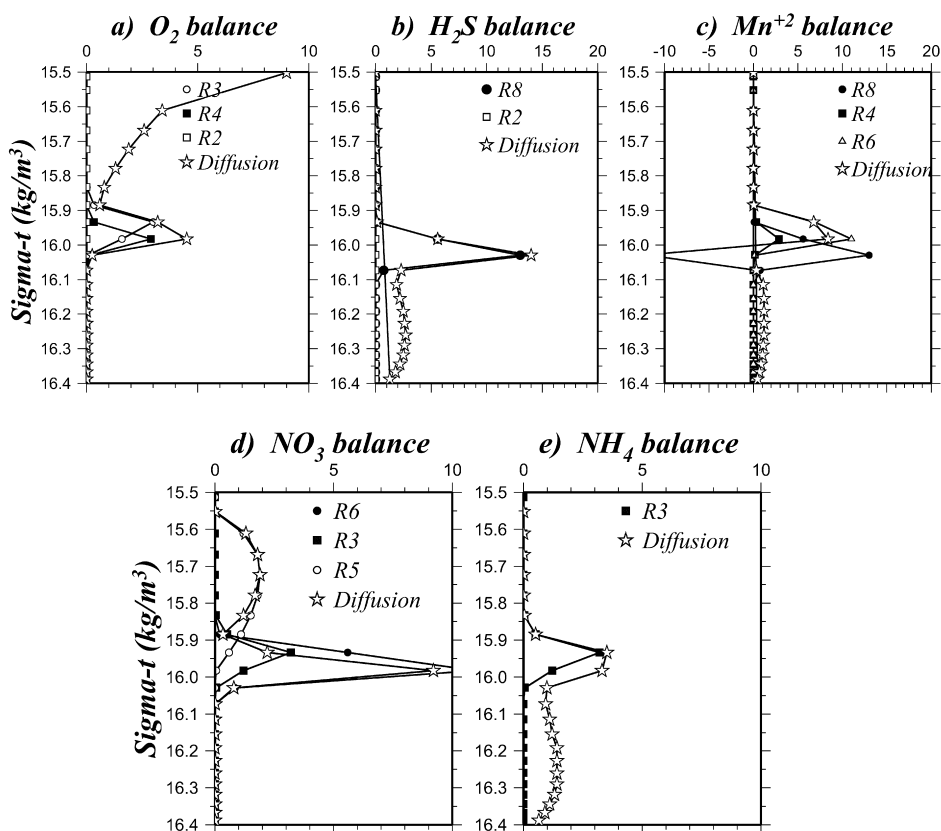


Fig. 6. Profiles of reactions (1)–(8) (in nM/d) plotted versus σ_t , showing the balances of (a) O₂, (b) H₂S, (c) Mn²⁺, (d) NO₃⁻, (e) NH₄⁺ equations for the standard experiment.

of magnitude smaller contribution. In the mass balance of hydrogen sulfide (Fig. 6b), the diffusion source term is balanced mainly by consumption by particulate manganese oxidation (8). The sink term representing sulfide oxidation by oxygen (2) is much smaller, as indicated above.

The reactions contributing to the dissolved manganese balance exhibit more complex vertical structure near the interface (Fig. 6c). Above $\sigma_t \sim 16.0$ kg/m³, the diffusion source term has a positive contribution to balance losses due to the Mn²⁺ oxidation with nitrate (6) and oxygen (4). Reaction (8) (oxidation of HS⁻ by MnO₂) has negligible contribution within this part of the interface zone. Below $\sigma_t \sim 16.0$ kg/m³, the main balance for Mn²⁺ occurs between diffusive loss and a source from Reaction (8). Reactions (4) and (6) also contribute to Mn²⁺ loss from the system to a lesser extent. On the other hand, contribution of (7) to the manganese balance is negligible throughout the water column, and therefore is not included in Fig. 6c. The particulate manganese balance is exactly the same as the Mn²⁺ balance except for the opposite signs. The sinking of MnO₂ has only a secondary contribution.

In the nitrate balance (Fig. 6d), the denitrification term (5) goes to zero near the upper boundary of the model when oxygen exceeds 5 μ M, and near $\sigma_t \sim 16.0$ kg/m³ when the NO₃⁻ concentration vanishes. This loss is compensated by the diffusive input of nitrate from the upper boundary of the

model up to $\sigma_t \sim 15.9 \text{ kg/m}^3$ and by nitrate production below due to the reaction (3) (ammonium oxidation with oxygen). Below $\sigma_t \sim 16.0 \text{ kg/m}^3$, the NO_3^- balance is maintained mainly by the diffusional source and dissolved manganese oxidation by nitrate (6). Reaction (3) is a secondary source term to this balance. Similarly, in the ammonium balance (Fig. 6e), ammonium oxidation by oxygen (3) is balanced by diffusion from deeper than $\sigma_t \sim 16.0 \text{ kg/m}^3$. Below $\sigma_t \sim 16.0 \text{ kg/m}^3$, the balance is between upward diffusion and ammonium oxidation by MnO_2 (7). Finally, we note that the total diffusive and reactive fluxes of dissolved oxygen and manganese agree reasonably well with those estimated from the observations shown in Figs. 12 and 14 of Lewis and Landing (1991). This agreement provides further confidence in the realism of the modeled reactions for representing redox reactions in the water column.

7.4. Experiments without contribution of oxygen

The experiments described in the previous sections indicate that NO_3^- rather than oxygen plays an important role in oxidizing H_2S and NH_4^+ . Here, we provide an additional experiment in which, as a limiting case, the redox reactions involving oxygen (i.e., Eqs. (2)–(4)) are excluded. This case investigates what the distributions would be if O_2 was not involved at all. The system is then governed only by Reactions (5)–(8). Thus, we set $k_2 = k_3 = k_4 = 0$; the rest of the parameters are same as in the standard experiment (cf. Experiment 4 in Table 3). Under these conditions, hydrogen sulfide is oxidized solely by particulate manganese, whose availability depends on the NO_3^- and Mn^{2+} concentrations within the interface zone.

As shown in Fig. 7, the main features of the suboxic–anoxic interface structure do not differ much from those for the standard experiment (Fig. 5). The lack of oxygen as an additional oxidizer is partially compensated by additional consumption of NO_3^- near the anoxic interface region. As a result, NO_3^- concentration tends to approach trace level values at a slightly shallower depth corresponding to $\sigma_t \sim 15.97 \text{ kg/m}^3$. This position also characterizes the trace level sulfide concentration and the elemental sulfur peak. The vertical displacement of this position is about $\Delta\sigma_t \sim 0.07 \text{ kg/m}^3$, which amounts to a depth difference of approximately 5 m. The position of particulate manganese is also elevated upwards by the same proportion. The change in the position of the suboxic–anoxic interface is also accompanied by an approximately 30% reduction in the peak concentrations of elemental sulfur and particulate manganese.

7.5. Experiments with lateral O_2 input

Recent observations performed east of the Bosphorus (Codispoti et al., 1991; Ozsoy et al., 1993; Basturk et al., 1998) suggest onshore–offshore exchanges and cross-shelf ventilation along the periphery of the Black Sea. They are most likely induced by meanders and complex eddy activities of the Rim Current system of the Black Sea general circulation, and therefore have transient character. An example of such quasi-lateral injection of oxygen rich shelf waters offshore towards the upper boundary of the hydrogen sulfide layer is shown in Fig. 8 on the basis of measurements carried out at a station along the topographic slope to the east of the Bosphorus during July 1997 (Basturk et al., 1998). The station was located inside an anticyclonic eddy, and the position of the sulfide boundary was therefore expected to be somewhat deeper as compared with those of offshore stations.

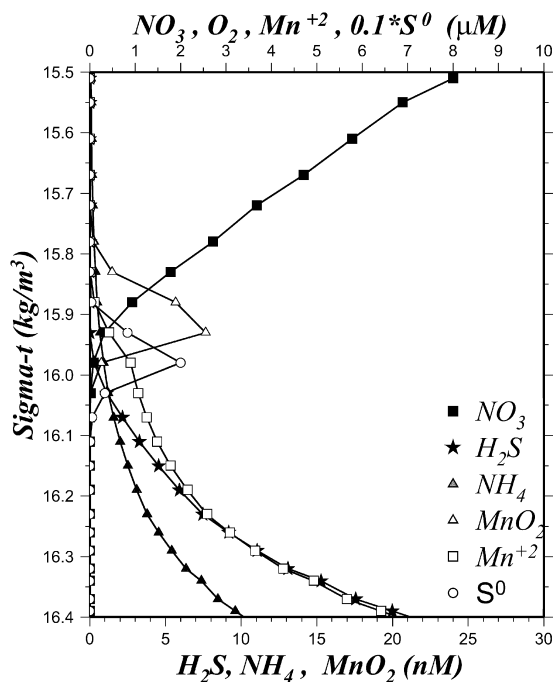


Fig. 7. HS^- , NH_4^+ , NO_3^- , S^0 , Mn^{2+} and MnO_2 profiles plotted versus σ_t for the case of no oxygen contribution to the redox reactions; i.e. $k_2 = k_3 = k_4 = 0$. (Experiment 4).

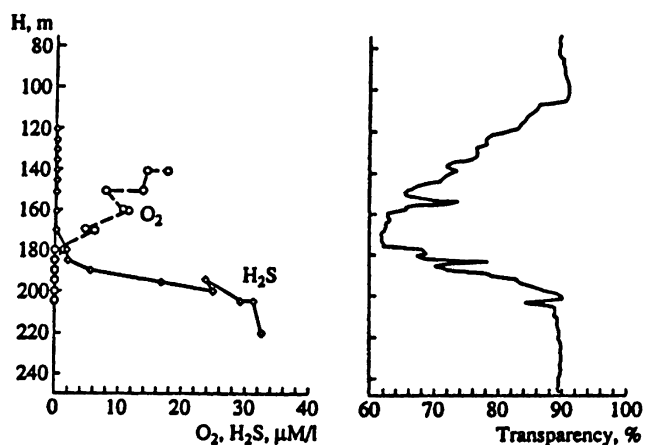


Fig. 8. Vertical distributions of dissolved oxygen, hydrogen sulfide (μM) and light transmission (%), at station $31^\circ 29' \text{E}$, $41^\circ 46' \text{N}$ during July 1997 RV *Bilim* measurements (after Basturk et al., 1998).

The presence of a deep light transmission minimum layer (Fig. 8a) between 110 and 180 m depths (corresponding to isopycnal surfaces of 15.9 and 16.4 kg/m^3) suggests offshore sediment transport from the shelf, and indicates presence of a fine particle layer (Kempe et al., 1991). This layer is also characterized by relatively higher dissolved oxygen concentrations of about 20 μM at 140 m depth

($\sigma_t \sim 16.2 \text{ kg/m}^3$), decreasing within the next 40 m to zero at the depth of the first appearance of hydrogen sulfide near $\sigma_t \sim 16.4 \text{ kg/m}^3$ (Fig. 8b). When compared with its typical position at offshore stations having oxygen and sulfide profiles as in Fig. 1b, both the trace oxygen concentration level and the upper boundary of the hydrogen sulfide layer are found to be located at deeper levels by about $\sigma_t \sim 0.2\text{--}0.25 \text{ kg/m}^3$. This structure, therefore, implies approximately 40 m erosion of the hydrogen sulfide layer due most likely to quasi-lateral injection of more oxygenated shelf waters offshore.

On the basis of these observations, an idealized experiment was designed to quantify possible contribution of transient lateral oxygen input to the suboxic zone structure around the periphery of the basin. In our one-dimensional model, the lateral oxygen supply was parameterized by the term $[F_L(\text{O}_2)]$ added on the right-hand side of Eq. (17). It was expressed as

$$F_L(\text{O}_2) = -u_s \frac{\partial [\text{O}_2]}{\partial x} \simeq \frac{u_s}{\Delta x} ([\text{O}_2]_s - [\text{O}_2]) \quad (25)$$

where u_s is the offshelf current speed taken as 0.1 m/s. Δx is the distance between the shelf and the location within the basin's interior where this model is applied. It was specified typically as 100 km. Oxygen supplied offshore from the near bottom levels of the shelf was set to $[\text{O}_2]_s = 3.0 \text{ }\mu\text{M}$ between $\sigma_t = 16.0$ and $\sigma_t = 16.25 \text{ kg/m}^3$ surfaces, corresponding to the depths of 105–125 m. Starting from the steady-state solution of the standard experiment (see Fig. 5) as the initial conditions, the structure of the suboxic–anoxic interface zone was simulated during 30 d of continuous lateral advective supply of oxygen. The conditions at the end of 15 and 30 d of oxygen input are shown in Figs. 9a and b. This experiment is listed as Experiment 5 in Table 3.

The local increase in the oxygen concentration associated with this lateral supply is clearly noted in Figs. 9a and b below the depth of $\sigma_t = 16.0 \text{ kg/m}^3$. The extra oxygen concentration takes part immediately in the H_2S oxidation process (Fig. 9a), and brings down the trace level H_2S concentration from its position at $\sigma_t = 16.05 \text{ kg/m}^3$ prior to the oxygen supply to $\sigma_t = 16.15 \text{ kg/m}^3$ after 15 d and to $\sigma_t = 16.25 \text{ kg/m}^3$ after 30 d of supply. Other modifications on the interface structure include increases in the elemental sulfur and particulate manganese concentrations by an order of magnitude. The maximum elemental sulfur concentration increased from about 0.3 to 3.0 μM and 5.0 μM in 15 and 30 d. Its position, coinciding with that of the zero- H_2S concentration level, was then located at deeper density levels. Particulate manganese concentration increases to approximately 300 nM after 15 d and 500 nM after 30 d of simulation. The enhanced particulate manganese stock generated locally according to Reaction (4) between $\sigma_t = 16.0$ and $\sigma_t = 16.25 \text{ kg/m}^3$ surfaces was then used to oxidize H_2S according to Reaction (8). The local dissolved manganese production associated with this reaction is seen in Figs. 9a and b from the local increase of Mn^{2+} concentration in the vicinity of the zero H_2S concentration level. This simulation therefore suggests that the lateral oxygen supplied to the interior of the basin from the peripheral zone may be used not only as a direct oxidizer for H_2S , but also indirectly through enhanced manganese cycling.

Clearly, the form of modified redox structure simulated in Figs. 9a and b depends on the duration and intensity of lateral oxygen supply. The structure in Fig. 9 characterizes the conditions of weak oxygen supply for a time period of several weeks representing typical time scale of slowly propagating mesoscale eddies and meanders passing through the region. On the other hand, both observed and simulated oxygen-sulfide profiles indicate that first appearance of hydrogen sulfide

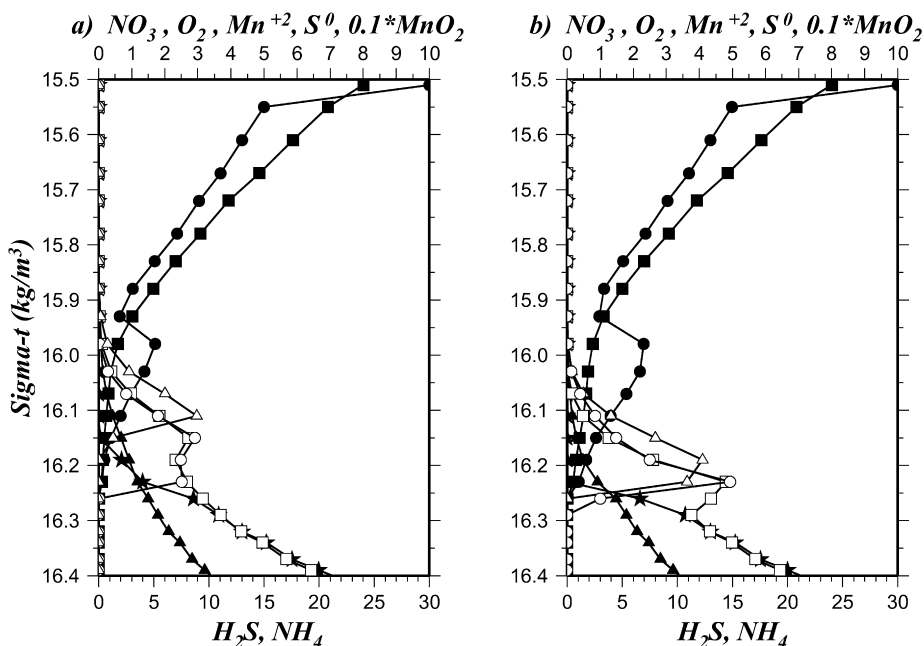


Fig. 9. O_2 (●), HS^- (★), NH_4^+ (▲), NO_3^- (■), S^0 (○), Mn^{2+} (□) and MnO_2 (△) profiles plotted versus σ_t for the standard experiment after (a) 15 d and (b) 30 d of continuous lateral oxygen supply with $[\text{O}_2]_s = 3.0 \mu\text{M}$ between $\sigma_t = 16.0$ and $\sigma_t = 16.25 \text{ kg/m}^3$ surfaces (Experiment 5).

coincides with the position of trace oxygen concentration, and that the suboxic layer vanishes under such conditions. However, oxygen and sulfide still do not overlap with each other and the co-existence layer does not form, even in the case of relatively strong oxygen injections as in the observations shown in Fig. 8b.

7.6. Sensitivity analysis

7.6.1. Different rate constants

An extensive set of experiments was conducted to explore dependency of the redox reactions on the rate constants. An important, and rather unexpected, finding from these experiments was the insensitivity of the distributions to the values of the rate constants. We found that order of magnitude changes in the rate constants did not appreciably affect the suboxic-anoxic interface structure. Because reactions R_6 , R_7 and R_8 govern the major features of the model, and are able to simulate several chemical gradients without reactions involving oxygen (see Fig. 7), we first present results with different settings of Experiment 4 described previously in Section 7.4. For example, the conditions shown in Fig. 10a for Experiment 6A (with $k_6 = 1.0 \mu\text{M}^{-1} \text{d}^{-1}$ and $k_8 = 500.0 \mu\text{M}^{-1} \text{d}^{-1}$) are quite similar to those shown in Fig. 7 for Experiment 4 with $k_6 = 0.05 \mu\text{M}^{-1} \text{d}^{-1}$ and $k_8 = 50.0 \mu\text{M}^{-1} \text{d}^{-1}$. The only noticeable difference is the relatively higher maximum concentration of particulate manganese, since Reaction (6) now allows more MnO_2 production in the water column. NO_3^- and H_2S profiles are also separated more clearly.

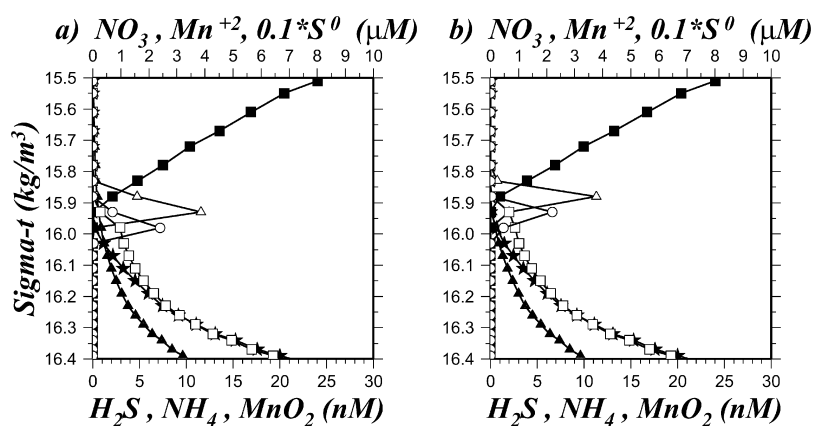


Fig. 10. HS⁻ (★), NH₄⁺ (▲), NO₃⁻ (■), S⁰ (○), Mn²⁺ (□) and MnO₂ (△) profiles plotted versus σ_t for the case of no oxygen contribution to the redox reactions and (a) with $k_6 = 1.0 \mu\text{M}^{-1} \text{d}^{-1}$, $k_8 = 500.0 \mu\text{M}^{-1} \text{d}^{-1}$ (Experiment 6A), and (b) with $k_6 = 1.0 \mu\text{M}^{-1} \text{d}^{-1}$, $k_8 = 500.0 \mu\text{M}^{-1} \text{d}^{-1}$, and $k_7 = 10.0 \mu\text{M}^{-1} \text{d}^{-1}$ (Experiment 6B).

When the value of k_7 was also increased from 0.1 to $10 \mu\text{M}^{-1} \text{d}^{-1}$ (see Experiment 6B in Table 3), resulting in a much faster oxidation rate of ammonium by particulate manganese, the structure remained the same but was elevated upwards by about 5 m or $\Delta\sigma_t \sim 0.05 \text{ kg/m}^3$ (Fig. 10b). The cause of this shift is more ammonium consumption within the suboxic layer and subsequently more dissolved manganese production according to Reaction (7). This dissolved manganese is oxidized by NO₃⁻ to produce particulate manganese, which eventually depletes more H₂S in the water column. More intense ammonium consumption is reflected by slight differences in the ammonium profiles in Figs. 10a and b.

We next describe a repetition of the standard experiment using $k_8 = 1.0 \mu\text{M}^{-1} \text{d}^{-1}$ as suggested by Yao and Millero (1993). This is called Experiment 6K in Table 3. An order of magnitude reduction in the value of k_8 led to a weakening of the role of manganese cycling in sulfide oxidation relative to that of vertical diffusion. Accordingly, H₂S penetrated up to $\sigma_t \sim 15.95 \text{ kg/m}^3$ (Fig. 11a) as compared to its original position at $\sigma_t \sim 16.05 \text{ kg/m}^3$ in Experiment 3. The maximum MnO₂ concentration at the interface region decreased by 35% to about $10 \mu\text{M}$. Reducing the role of manganese oxidation on hydrogen sulfide is better shown if the contribution from oxygen oxidation is isolated from the system. Thus, Experiment 6K was repeated under the conditions of $k_2 = k_3 = k_4 = 0$, as indicated by Experiment 6L in Table 3. Under these conditions, the position of the zero hydrogen sulfide concentration was elevated further up to $\sigma_t \sim 15.80 \text{ kg/m}^3$ (Fig. 11b). Because of the absence of Reaction (4), particulate manganese concentration also decreased to half of its value in Experiment 6K.

7.6.2. Different A_v and W_s

The effect of changes in the diffusion coefficient and sinking rate of manganese particles (see Experiments 7A–C in Table 3) on the “standard experiment” are displayed in Figs. 11a and b. Increasing the diffusion coefficient from 2 to $4 \times 10^{-6} \text{ m}^2/\text{s}$ (Experiment 7A) elevates the zero concentration levels of NH₄⁺, H₂S and Mn²⁺ slightly upwards (Fig. 12a). This also allows more

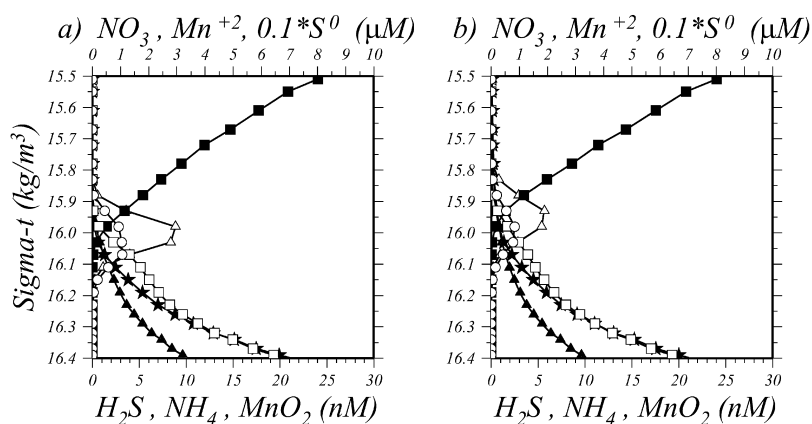


Fig. 11. HS^- (\star), NH_4^+ (\blacktriangle), NO_3^- (\blacksquare), S^0 (\circ), Mn^{2+} (\square) and MnO_2 (\triangle) profiles plotted versus σ_t for the standard experiment except with reduced sulfide oxidation rate by particulate manganese (a) $k_8 = 1.0 \mu\text{M}^{-1} \text{d}^{-1}$ (Experiment 6K), and (b) $k_8 = 1.0 \mu\text{M}^{-1} \text{d}^{-1}$ together with $k_2 = k_3 = k_4 = 0$. (Experiment 6L).

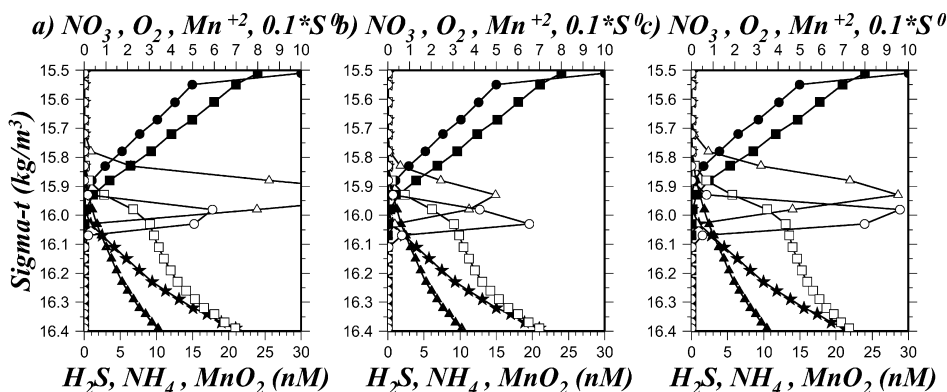


Fig. 12. O_2 (\bullet), HS^- (\star), NH_4^+ (\blacktriangle), NO_3^- (\blacksquare), S^0 (\circ), Mn^{2+} (\square) and MnO_2 (\triangle) profiles plotted versus σ_t for the standard experiment except with (a) $A_v = 4 \times 10^{-6} \text{m}^2/\text{s}$ (Experiment 7A), (b) $W_s = 9 \text{m/d}$ (Experiment 7B), and (c) $A_v = 6 \times 10^{-6} \text{m}^2/\text{s}$, and $W_s = 9 \text{m/d}$ (Experiment 7C).

diffusive influx of oxygen and nitrate into the interface zone, which results in higher reaction rates for these oxidants. Consequently, oxygen and nitrate vanish at slightly deeper levels. The position of the particulate manganese peak is elevated upwards and its magnitude doubled as compared with the standard experiment shown in Fig. 5. The change in the sinking rate of manganese oxide particles from 3 to 9 m/d (Experiment 7B) did not alter the interface structure much, except for a reduction in the maximum MnO_2 concentration with a slight increase in the dissolved manganese concentration within the interface zone (Fig. 12b). For the higher value of particulate manganese sinking rate ($W_s = 9 \text{m/d}$), a further increase in the diffusion coefficient to $A_v = 6 \times 10^{-6} \text{m}^2/\text{s}$ (Experiment 7C) shifted the position of the vanishing oxygen and nitrate concentrations as well as the particulate manganese peak upwards (Fig. 12c). The maximum

concentrations of MnO_2 and elemental sulfur increase to some extent as well. But, the general structure of the suboxic–anoxic interface zone remains fairly similar and therefore does not depend crucially on the changes in the values of A_v and W_s within their expected range.

8. Summary and concluding remarks

A prognostic, one-dimensional vertically resolved diffusion-reaction model was described to investigate reactions and factors controlling the suboxic–anoxic interface structure in the Black Sea. The model included a simplified system of redox cycling characterized by nitrogen and sulfur reactions catalyzed by manganese cycling. In oxygen depleted waters, the model suggests that oxidation-reduction processes occur via manganese cycling. Dissolved manganese reacts with nitrate to produce settling particulate manganese dioxide and nitrogen gas. The upward fluxes of sulfide and ammonium are oxidized by particulate manganese to form elemental sulfur, nitrogen gas and dissolved manganese. Elemental sulfur is then reduced back to sulfide by bacteria, whereas dissolved manganese produced locally contributes further to the nitrate oxidation process. Although fairly simplified and idealized, these reactions form a coupled and highly interactive system successfully describing redox processes in the Black Sea.

Reactions were expressed in terms of second-order kinetics in which the values of rate constants were constrained by available rate measurements. The model was calibrated by specific data sets obtained during the 1988 RV *Knorr* cruises. The goal of the calibration exercise was not to reproduce the best fits to the observed profiles, but to see if these reactions can simulate the major features and to generate a set of adjusted parameter values for the model. For simplicity, the model was decoupled from the euphotic zone processes of plankton production and organic matter generation. Its upper boundary was located at $\sigma_t \sim 15.5 \text{ kg/m}^3$, where it was forced by prescribed nitrate and oxygen concentrations. The lower boundary was specified inside the anoxic pool at $\sigma_t \sim 16.5 \text{ kg/m}^3$. Hydrogen sulfide, ammonium and dissolved manganese concentrations were prescribed at this boundary. Following a few years of transient adjustment, the system evolved to an equilibrium state governed by the set of reactions specified in the model.

A series of simulations was performed to explore contributions of different reactions to the structure of the suboxic–anoxic interface. The experiments included: (i) dissolved oxygen considered as the only oxidizer without any role of manganese cycling, (ii) the reverse case with particulate manganese dioxide acting as the main oxidizing agent without any reactions with oxygen, (iii) fully active manganese cycling in which both dissolved oxygen and particulate manganese control the redox environment, and (iv) cross-shelf advection of oxygen injected quasi-laterally and temporally into the interface region.

The experiments with dissolved oxygen as the only oxidizer predicted the position of the trace sulfide concentrations at $\sigma_t \leq 15.9 \text{ kg/m}^3$, which is approximately 10 m shallower than its observed level at $\sigma_t \sim 16.1 \text{ kg/m}^3$ (see Figs. 3 and 4). These distributions support the conclusion that hydrogen sulfide and oxygen cannot co-exist under normal conditions. In the case of fully active manganese cycling, the model simulated the suboxic layer structure with oxygen concentrations less than $5 \mu\text{M}$ and zero sulfide concentrations between $\sigma_t \sim 15.55 \text{ kg/m}^3$ and $\sigma_t \sim 16.05 \text{ kg/m}^3$ surfaces (Fig. 5). Dissolved oxygen decreased to trace concentrations above the zone of nitrate

reduction. Dissolved manganese and ammonium then increased downward into deeper levels of the anoxic pool. Hydrogen sulfide followed the same trend starting from the position where the nitrate became undetectable. This zone located in the vicinity of $\sigma_t \sim 16.0 \text{ kg/m}^3$ was also characterized by a particulate manganese peak reflecting paramount role of manganese cycling in the redox processes.

Oxygen alone could not provide a realistic interface structure in the absence of particulate manganese generated by oxidation of Mn^{2+} with nitrate. On the other hand, the main features of the interface structure do not change much when oxygen is not used as an oxidizer (Fig. 7). In this case, the lack of oxygen is partially compensated by additional consumption of nitrate near the anoxic interface zone. A transient lateral oxygen supply into sulfide rich waters immediately below the interface zone rapidly depleted the local hydrogen sulfide layer, thus temporally altering the anoxic-suboxic interface region (Fig. 9). The sensitivity experiments suggest that the main features of the suboxic–anoxic interface region were not highly sensitive to the values of the rate constants of the reactions. We actually know quite little about the mechanisms and rates of these reactions. The model results therefore may improve our understanding of redox cycling across the suboxic–anoxic interface zone of the Black Sea in particular, and of similar marine systems in general.

The model simulations indicate that the set of reactions described by Eqs. (1)–(8) can simulate the main features of the suboxic–anoxic interface zone, and provide quantitative evidence for the presence of an oxygen and sulfide depleted suboxic zone. It appears that the downward supply of nitrate from the overlying nitracline zone and the upward transport of dissolved manganese from the anoxic pool below are crucially important for maintenance of the suboxic layer. Interaction of nitrate and dissolved manganese with each other near the $\sigma_t \sim 16.0 \text{ kg/m}^3$ level is the mechanism that triggers the redox reactions and gives rise to observed vertical profiles of O_2 , NO_3^- , NH_4^+ , HS^- , S^0 , Mn^{2+} , MnO_2 .

In this first exploratory attempt investigating the dynamics of the suboxic zone, our attention was restricted only to understanding the basic structural characteristics of the suboxic–anoxic interface. Further studies are necessary to elaborate the model in several directions. One particularly important research issue is to investigate whether or not the suboxic structure undergoes seasonal or shorter term (e.g. weekly) variabilities associated with various physical and biogeochemical processes. This requires coupling of the model with a dynamical model and with a biogeochemical model including biological production and organic matter generation and settling within the upper part of water column. Moreover, addition of a more complex sulfur cycle, of iron cycling, and of anoxygenic photosynthesis are expected to lead to further improvements and a more complete representation of the suboxic–anoxic interface system. Other types of oxidation-reduction reactions thought to occur in this zone could also be tested by the model.

Acknowledgements

This work is a contribution to ODBMS-Black Sea project, sponsored by the NATO Science for Peace Program. T. Oguz acknowledges partial support by NSF Grant OCE9906656 and NATO Linkage Grant EST.CLG975821.

References

- Aller, R.C., Hall, P.O.J., Rude, P.D., Aller, Y.J., 1998. Biogeochemical heterogeneity and suboxic diagenesis in hemipelagic sediments of the Panama Basin. *Deep-Sea Research I* 45, 133–165.
- Basturk, O., Saydam, C., Salihoglu, I., Eremeeva, L.V., Konovalov, S.K., Stoyanov, A., Dimitrov, A., Cociasu, A., Dorogan, L., Altabet, M., 1994. Vertical variations in the principle chemical properties of the Black Sea in the autumn of 1991. *Marine Chemistry* 45, 149–165.
- Basturk, O., Tugrul, S., Konovalov, S., Salihoglu, I., 1997. Variations in the vertical structure of water chemistry within the three hydrodynamically different regions of the Black Sea. In: Ozsoy, E., Mikaelyan, A. (Eds.), *Sensitivity to Change: Black Sea, Baltic Sea and North Sea*, NATO ASI Series 2, Environment, Vol. 27. Kluwer Academic Publishers, Dordrecht, pp. 183–196.
- Basturk, O., Volkov, I.I., Gokmen, S., Gungor, H., Romanov, A.S., Yakushev, E.V., 1998. International expedition on board R.V. Bilim in July 1997 in the Black Sea. *Oceanology (English translation)* 38, 429–432.
- Belyaev, V.I., Sovga, E.E., Lyubartseva, S.P., 1997. Modelling the hydrogen sulfide zone of the Black Sea. *Ecological Modelling* 13, 51–59.
- Boudreau, B., Mucci, A., Sundby, B., Luther, G.W., Silverberg, N., 1998. Comparative diagenesis at three sites on the Canadian continental margin. *Journal of Marine Research* 56, 1259–1284.
- Boudreau, P.B., 1996. A method-of-lines code for carbon and nutrient diagenesis in aquatic sediments. *Computer & Geosciences* 22, 479–496.
- Brewer, P.G., Spencer, D.W., 1974. Distribution of some trace elements in the Black Sea and their flux between dissolved and particulate phases. In: Degens, E.T., Ross, D.A. (Eds.), *The Black Sea- Geology, Chemistry, and Biology*. Vol. 20. The American Association of Petroleum Geologists, Memoir, pp. 137–143.
- Buesseler, K.O., Livingston, H.D., Ivanov, L., Romanov, A., 1994. Stability of the oxic-anoxic interface in the Black Sea. *Deep Sea Research* 41, 283–296.
- Burdige, D.J., Neelson, K.H., 1986. Chemical and microbiological studies of sulfide-mediated manganese reduction. *Geomicrobiology Journal* 4, 361–387.
- Codispoti, L.A., Friederich, G.E., Murray, J.W., Sakamoto, C.M., 1991. Chemical variability in the Black Sea: implications of continuous vertical profiles that penetrated the oxic/anoxic interface. *Deep-Sea Research I* 38 (Suppl. 2A), S691–S710.
- Eremeev, V.N., 1996. Hydrochemistry and dynamics of the hydrogen-sulfide zone in the Black Sea. In: Griffiths, R.C. (Ed.), *Unesco Reports in Marine Science*, UNESCO, 1996, Paris, 114pp.
- Faschuk, D.Ya., Ayzatullin, T.A., Dronov, V.V., Pankratova, T.M., Finkelshteyn, M.S., 1990. Hydrochemical structure of the layer of co-existence of oxygen and hydrogen sulfide in the Black Sea and a possible mechanism of its generation. *Oceanology (English translation)* 30, 185–192.
- Gargett, A.E., 1984. Vertical eddy diffusivity in the ocean interior. *Journal of Marine Research* 42, 359–393.
- Gokmen, S., Romanov, A.S., Basturk, O., Konovalov, S., 1998. A comparative study of spectrophotometric and iodometric back titration methods for hydrogen sulfide determination in anoxic Black Sea waters. In: Ivanov, L., Oguz, T. (Eds.), *Ecosystem Modeling as a Management Tool for the Black Sea*, Vol. 1, NATO ASI Series, 2 — Environmental Security, Vol. 47. Kluwer Academic Publishers, Dordrecht, pp. 55–64.
- Grashoff, K., 1975. The hydrochemistry of landlocked basins and fjords. In: Riley, J.P., Skirrow, C. (Eds.), *Chemical Oceanography*. Academic Press, New York, pp. 456–497.
- Gregg, M.C., Ozsoy, E., 1999. Mixing on the Black Sea shelf north of the Bosphorus. *Geophysical Research Letters* 26, 1869–1872.
- Hulth, S., Aller, R.C., Gilbert, F., 1999. Coupled anoxic nitrification/manganese reduction in marine sediments. *Geochimica et Cosmochimica Acta* 63, 49–66.
- Ivanov, L.I., Oguz, T., 1998. *Ecosystem Modeling as a Management Tool for the Black Sea*, Vol. 1 and 2, NATO ASI Series 2–47, Kluwer Academic Publishers, Dordrecht.
- Jahnke, R.A., 1998. Geochemical impacts of waste disposal on the abyssal seafloor. *Journal of Marine Systems* 14, 355–375.
- Jannasch, H.W., Wirsén, C.O., Molyneux, S.J., 1991. Chemoautotrophic sulfur-oxidizing bacteria from the Black Sea. *Deep-Sea Research* 38 (Suppl. 2A), S1105–S1120.

- Jorgensen, B.B., Fossing, H., Wirsén, C.O., Jannasch, H.W., 1991. Sulfide oxidation in the anoxic Black Sea chemocline. *Deep-Sea Research* 38 (Suppl. 2A), S1083–S1104.
- Karl, D.M., 1978. Distribution, abundance and metabolic states of microorganisms in the water column and sediments of the Black Sea. *Limnology and Oceanography* 23, 936–949.
- Karl, D.M., Knauer, G.A., 1991. Microbial production and particle flux in the upper 350 m of the Black Sea. *Deep Sea Research* 38 (Suppl. 2A), S655–S661.
- Kempe, S., Diercks, A.R., Liebezeit, G., Prange, A., 1991. Geochemical and structural aspects of the pycnocline in the Black Sea (R/V *Knorr* 134–8 Leg 1, 1988). In: Izdar, E., Murray, J.W. (Eds.), *Black Sea Oceanography*, NATO ASI Series C, Vol. 351. Kluwer Academic Publishers, Dordrecht, pp. 89–110.
- Konovalov, S., Tugrul, S., Basturk, O., Salihoglu, I., 1997. Spatial isopycnal analysis of the main pycnocline chemistry of the Black Sea. In: Ozsoy, E., Mikaelyan, A. (Eds.), *Sensitivity to Change: Black Sea, Baltic Sea and North Sea*, NATO ASI Series 2, Environment, Vol. 27. Kluwer Academic Publishers, Dordrecht, pp. 197–210.
- Konovalov, S.K., Ivanov, L.I., Murray, J.W., Ereemeeva, L.V., 1999. Eutrophication: a plausible cause for changes in hydrochemical structure of the Black Sea anoxic layer. In: Besiktepe, S.T., Unluata, U., Bologna, A.S. (Eds.), *Environmental Degradation of the Black Sea: Challenges and Remedies*, NATO ASI Series 2–56. Kluwer Academic Publishers, Dordrecht, pp. 61–74.
- Lewis, B.L., Landing, W.M., 1991. The biogeochemistry of manganese and iron in the Black Sea. *Deep-Sea Research* 38 (Suppl. 2A), S773–S804.
- Lipschultz, F., Wofsy, S.C., Ward, B.B., Codispoti, L.A., Friedrich, G., Elkins, J.W., 1990. Bacterial transformations of inorganic nitrogen in the oxygen-deficient waters of the Eastern Tropical South Pacific Ocean. *Deep-Sea Research* 37, 1513–1541.
- Luther III, G.W., Sundby, B., Lewis, B.L., Brendel, P.J., Silverberg, N., 1997. The interaction of manganese with the nitrogen cycle in continental margin sediments: Alternative pathways for dinitrogen formation. *Geochimica et Cosmochimica Acta* 61, 4043–4052.
- Lyubartseva, S.P., Lyubartsev, V.G., 1998. Modeling of the Black Sea anoxic zone processes. In: Ivanov, L., Oguz, T. (Eds.), *Ecosystem Modeling as a Management Tool for the Black Sea*, Vol. 2., NATO ASI Series, 2 — Environmental Security, Vol. 47. Kluwer Academic Publishers, Dordrecht, pp. 385–396.
- Mellor, G.L., 1990. User's guide for a three dimensional, primitive equation numerical ocean model. *Progress in Atmospheric and Ocean Science*. Princeton University, Princeton, NJ, 35pp.
- Millero, F.J., Hubinger, S., Fernandez, M., Garnett, S., 1987. The oxidation of H₂S in seawater as a function of temperature, pH and ionic strength. *Environmental Science and Technology* 21, 439–443.
- Millero, F.J., 1991. The oxidation of H₂S in the Black Sea waters. *Deep-Sea Research* 38 (Suppl. 2A), S1139–S1150.
- Murray, J.W., Jannasch, H.W., Honjo, S., Anderson, R.F., Reeburgh, W.S., Top, Z., Friederich, G.E., Codispoti, L.A., Izdar, E., 1989. Unexpected changes in the oxic/anoxic interface in the Black Sea. *Nature* 338, 411–413.
- Murray, J.W., 1991. Black Sea oceanography: results from the 1988 Black Sea expedition. *Deep-Sea Research* 38 (Suppl. 2A), 1266.
- Murray, J.W., Codispoti, L.A., Friederich, G.E., 1995. Oxidation-reduction environments: the suboxic zone in the Black Sea. In: Huang, C.P., O'Melia, C.R., Morgan, J.J. (Eds.), *Aquatic Chemistry: Interfacial and Interspecies Processes*. ACS Advances in Chemistry Series No. 224. pp. 157–176.
- Murray, J.W., Lee, B.S., Bullister, J., Luther III, G.W., 1999. The suboxic zone of the Black Sea. In: Besiktepe, S., Unluata, U., Bologna, A. (Eds.), *Environmental Degradation of the Black Sea: Challenges and Remedies*. NATO ASI Series 2–56. Kluwer Academic Publishers, Dordrecht, pp. 75–92.
- Myers, C., Nealson, K., 1988. Bacterial manganese reduction and growth with manganese oxide as the sole electron acceptor. *Science* 240, 1319–1321.
- Nealson, K.H., Myers, C.R., Wimpee, B.B., 1991. Isolation and identification of manganese-reducing bacteria and estimates of microbial Mn(IV)-reducing potential in the Black Sea. *Deep-Sea Research* 38 (Suppl. 2A), S907–S920.
- Oguz, T., Latun, V.S., Latif, M.A., Vladimirov, V.V., Sur, H.I., Makarov, A.A., Ozsoy, E., Kotovshchikov, B.B., Ereemeev, V.V., Unluata, U., 1993. Circulation in the surface and intermediate layers of the Black Sea. *Deep-Sea Research I* 40, 1597–1612.
- Oguz, T., Ducklow, H.W., Malanotte-Rizzoli, P., Tugrul, S., Nezhlin, N., Unluata, U., 1996. Simulation of annual plankton productivity cycle in the Black Sea by a one-dimensional physical-biological model. *Journal Geophysical Research* 101, 16 585–16 599.

- Oguz, T., Ducklow, H.W., Shuskina, E.A., Malanotte-Rizzoli, P., Tugrul, S., Lebedeva, L.P., 1998a. Simulation of upper layer biogeochemical structure in the Black Sea. In: Ivanov, L., Oguz, T. (Eds.), *Ecosystem Modeling as a Management Tool for the Black Sea*, Vol. 2. NATO ASI Series, 2 — Environmental Security, Vol. 47. Kluwer Academic Publishers, Dordrecht, pp. 257–300.
- Oguz, T., Ducklow, H.W., Malanotte-Rizzoli, P., Murray, J.W., 1998b. Simulations of the Black Sea pelagic ecosystem by one dimensional vertically resolved physical-biochemical models. *Fisheries Oceanography* 7, 300–304.
- Oguz, T., Ducklow, H.W., Malanotte-Rizzoli, P., Murray, J.W., Vedernikov, V.I., Unluata, U., 1999. A physical-biochemical model of plankton productivity and nitrogen cycling in the Black Sea. *Deep-Sea Research I* 46, 597–636.
- Ozsoy, E., Unluata, U., Top, Z., 1993. The evolution of Mediterranean water in the Black Sea: Interior mixing and material transport by double diffusive intrusions. *Progress in Oceanography* 31, 275–320.
- Repeta, D.J., Simpson, D.J., 1991. The distribution and recycling of chlorophyll, bacteriochlorophyll and carotenoids in the Black Sea. *Deep-Sea Research* 38 (Suppl. 2A), S969–S984.
- Repeta, D.J., Simpson, D.J., Jorgensen, B.B., Jannasch, H.W., 1989. Evidence for anoxic photosynthesis from the distribution of bacteriochlorophylls in the Black Sea. *Nature* 342, 69–72.
- Rozanov, A.G., Neretin, L.N., Volkov, I.I., 1998. Redox Nepheloid Layer (RNL) of the Black Sea: its location, composition and origin.. In: Ivanov, L., Oguz, T. (Eds.), *Ecosystem Modeling as a Management Tool for the Black Sea*, Vol. 1. NATO ASI Series, 2 — Environmental Security, Vol. 47. Kluwer Academic Publishers, Dordrecht, pp. 77–92.
- Saydam, C., Tugrul, S., Basturk, O., Oguz, T., 1993. Identification of the oxic/anoxic interface by isopycnal surfaces in the Black Sea. *Deep Sea Research* 40, 1405–1412.
- Schultz, H.D., Dahmke, A., Schinzel, T., Wallmann, K., Zabel, M., 1994. Early diagenetic processes, fluxes, and reaction rates in sediments of the South Atlantic. *Geochimica et Cosmochimica Acta* 58, 2041–2060.
- Shaw, T., Jahnke, R., Gieskes, J., 1990. Early diagenesis in differing depositional environments: the response of transition metals in pore water. *Geochimica et Cosmochimica Acta* 54, 1233–1246.
- Soetaert, K., Herman, P.M.J., Middelburg, J.J., 1996. A model of early diagenetic processes from shelf to abyssal depths. *Geochimica et Cosmochimica Acta* 60, 1019–1040.
- Sorokin, Y.I., 1972. The bacterial population and the process of hydrogen sulfide oxidation in the Black Sea. *Journale Conseil Internationale pour l'Exploration de la Mer* 34, 423–454.
- Spencer, D.W., Brewer, P.G., 1971. Vertical advection, diffusion and redox potentials as controls on the distribution of manganese and other trace metals dissolved in waters of the Black Sea. *Journal of Geophysical Research* 76, 5877–5892.
- Tebo, B.M., 1991. Manganese (II) oxidation in the suboxic zone of the Black Sea. *Deep-Sea Research* 38 (Suppl. 2A), S883–S906.
- Tebo, B.M., Rosson, R.A., Neilson, K.H., 1991. Potential for manganese (II) oxidation and manganese (IV) reduction to co-occur in the suboxic zone of the Black Sea. In: Izdar, E., Murray, J.W. (Eds.), *Black Sea Oceanography*, NATO ASI Series C, Vol. 351. Kluwer Academic Publishers, Dordrecht, pp. 173–186.
- Tugrul, S., Basturk, O., Saydam, C., Yilmaz, A., 1992. The use of water density values as a label of chemical depth in the Black Sea. *Nature* 359, 137–139.
- Vinogradov, M.E., Nalbandov, Yu.R., 1990. Effect of changes in water density on the profiles of physicochemical and biological characteristics in the pelagic ecosystem of the Black Sea. *Oceanology (English translation)* 30, 567–573.
- Wang, Y., Cappellen, P.V., 1996. A multicomponent reactive transport model of early diagenesis: Application to redox cycling in coastal marine sediments. *Geochimica et Cosmochimica Acta* 60, 2993–3014.
- Ward, B.B., Kilpatrick, K.A., 1991. Nitrogen transformations in the oxic layer of permanent anoxic basins: The Black Sea and Cariaco Trench. In: Izdar, E., Murray, J.W. (Eds.), *Black Sea Oceanography*, NATO ASI Series C, Vol. 351. Kluwer Academic Publishers, Dordrecht, pp. 111–124.
- Yakushev, E.V., 1998. Mathematical modeling modeling of oxygen, nitrogen, sulfur and manganese cycling in the Black Sea. In: Ivanov, L., Oguz, T. (Eds.), *Ecosystem Modeling as a Management Tool for the Black Sea*, Vol. 2. NATO ASI Series, 2 — Environmental Security, Vol. 47. Kluwer Academic Publishers, Dordrecht, pp. 373–384.
- Yakushev, E.V., Neretin, L.N., 1997. One dimensional modeling of nitrogen and sulfur cycles in the aphotic zone of the Black and Arabian Seas. *Global Biogeochemical Cycles* 11, 401–414.
- Yao, W., Millero, F.J., 1993. The rate of sulfide oxidation by MnO₂ in seawater. *Geochimica et Cosmochimica Acta* 57, 3359–3365.